Ordered spin structures of β-MnO$_2$ (rutile-type) systems with competing exchange interactions: numerical approach using equipotential contour plot

Masatsugu Suzuki[*] and Itsuko S. Suzuki[†]

Department of Physics, State University of New York at Binghamton, Binghamton, New York 13902-6016

(Dated: December 7, 2009)

Using numerical calculations of equi-energy contour plot of the Fourier transform of the spin Hamiltonian, we study the magnetic phase diagram (J_2 and J_3) of the rutile type β-MnO$_2$, where J_1 (< 0) is fixed and is the antiferromagnetic interaction along the diagonal direction, J_2 is the interaction along the c axis, and J_3 is the interaction along the a axis. The magnetic phase diagram consists of the multicritical point (the intersection $J_2 J_3 = J_1^2$ and $J_2 + J_3 = 2J_1$), the helical order along the c axis, the ($h = 1/2, k = 0, l = 1/2$) phase, the helical order along the a axis, and the phase ($h = 0, k = 0, l = 1$). The shift of the location of the magnetic Bragg peak in the ($h, 0, l$) reciprocal lattice plane is examined with the change of J_2 and J_3 in the magnetic phase diagram. The shift is continuous on the first-order phase transition, and is discontinuous on the second-order phase transition. The detail of our magnetic phase diagram is rather different from that reported by Yoshimori.

I.   INTRODUCTION

It is well known that β-MnO$_2$ (with the rutile-type structure) is one of the systems with a helical spin order along the c axis. Erickson[1] found from magnetic neutron scattering on β-MnO$_2$ that the helical spin order with a period of $7c$ along the c axis. The direction of spins in the c plane turns from one plane to the next plane by an angle of $129°$ ($5\pi/7$). In 1958, Yoshimori[2] theoretically demonstrated the origin and stability of the helical spin order in β-MnO$_2$, based on the experimental results from Erickson. The spin Hamiltonian of β-MnO$_2$ is described by a form of the Heisenberg-type, where the combination of n.n. exchange interactions, n. n. n. exchange interactions, and son on are included. His success lies in the use of the Fourier transform of the spin Hamiltonian in the reciprocal lattice space. Then the Fourier transform depends only on exchange interactions and wavevectors $\mathbf{Q}$. The location of the magnetic Bragg points in the reciprocal lattice space are uniquely determined from the condition that the Fourier transform takes a maximum.

In spite of the success in theory established by Yoshimori,[1] Erickson has not published his detailed data of the magnetic neutron scattering of β-MnO$_2$ as far as we know. Since 1958, there have been several papers on the magnetic structure of β-MnO$_2$ using magnetic neutron scattering[3–5] and magnetic x-ray scattering.[6,7] In recent years, Sato et al, have reported that the magnetic Bragg peaks appear at the wave vector $\mathbf{Q} = (1, 0, 2 + \epsilon)$ in the units of a^* ($= 2\pi/a$), b^* ($= 2\pi/b$), and c^* ($= 2\pi/c$) in the reciprocal lattice space, where $\epsilon = 0.297$ at 10 K, increases with increasing temperature, and reaches 0.2992 just below T_N ($= 92$ K). The value of ϵ is rather different from $2/7$ derived by Yoshimori.[1] This indicates that the helical spin structure along the c axis is incommensurate with the c- axis lattice constant.

Because of the crystal field (distorted octahedron formed by O^{2-} ions) in the vicinity of Mn^{4+} ion, the ground orbital state of Mn^{4+} ion ($3d^3$, $L = 3$ and $S = 3/2$) is split into the t_{2g} ($d\epsilon$) level (lower energy level, triple degenerate) and the e_g ($d\gamma$) level (upper energy, double degenerate). As a result, the ground state is now orbital singlet, indicating that the orbital angular momentum is quenched. The e_g electrons are responsible for the metallic conduction, while the localized t_{2g} electrons are responsible for the magnetism. In recent years, Sato et al.[8] have reported the transport properties of a single crystal β-MnO$_2$, such as electrical resistivity, thermopower, Hall effect, and magnetoresistance. Their data show an appreciable anomaly near T_N. This implies that there is a strong correlation between conduction ϵ_g electrons and localized t_{2g} magnetic moment through the Hund's rule. The DC magnetic susceptibility shows a significant deviation from a molecular-field theory based on a localized spin model, which was assumed by Yoshimori[1] on his helical spin order.

In the present paper, we study the magnetic phase diagram of β-MnO$_2$ type structure using the molecular field theory developed by Yoshimori,[1] where Mn^{4+} spins are localized. The exchange interactions J_1 along the diagonal axis of the system, J_2 along the c axis and J_3 along the a axis are taken into account. Note that J_1 is assumed to be fixed and be antiferromagnetic. According to Sato et al.,[8] the intra-atomic $t_{2g}-e_g$ exchange interaction (Hund coupling), the transfer interaction between adjacent e_g orbitals, and the occupancy of the e_g orbitals are defined by J_{Hund}, t, and c, respectively. Since $|J_n| \gg |cJ_{Hund}|$ and $|J_n| \gg |ct|$ for β-MnO$_2$ ($n = 1,2,3$),[8] this means that the spin structure of β-MnO$_2$ below T_N is not affected by the effect of cJ_{Hund} and ct at al. In other words, the spin structure is well described by the localized spin model with J_1, J_2, and J_3. We find that our magnetic phase diagram (J_2 vs J_3) consists of four phases including the helical phase along the c axis, the phase with (1/2, 0, 1/2), the helical phase along the axis, and the phase with (1, 0, 0). The detail of our phase diagram is rather

different from that proposed by Yoshimori.[1] We use a numerical calculation approach in finding the distribution of the magnetic Bragg peaks in the fixed reciprocal lattice planes such as (h, k, l) with one index fixed. To this end we calculate the equi-energy contour plot of the negative sign of the Fourier transform of the spin Hamiltonian, $J(h, k, l)$. The magnetic Bragg peaks are located inside the maximum equi-energy contour. The selection rule for the location of the magnetic Bragg peaks is the same as that derived by Yoshimori.[1] This numerical method has an advantage in visualizing the location of the magnetic Bragg peaks in the reciprocal lattice space. The nature of the phase transitions on the phase boundaries will be discussed.

II. BACKGROUND: GENERAL THEORY FOR THE ORDERED SPIN STRUCTURE

We follow the theory presented by Nagamiya.[9] We consider a lattice of magnetic atoms such as β-MnO_2. The unit cell can be chosen so that it contains one magnetic atom. On each magnetic atom, we assume a *classical spin*. Between the spin $\mathbf{S}_i$ at the position $\mathbf{R}_i$ and $\mathbf{S}_j$ at $\mathbf{R}_j$, there is an Heisenberg-type exchange interaction. The Heisenberg spin Hamiltonian is expressed by

$$H = -2 \sum_{i,j} J(\mathbf{R}_{ij}) \mathbf{S}_i \cdot \mathbf{S}_j, \tag{1}$$

where

$$J(-\mathbf{R}_{ij}) = J(\mathbf{R}_{ij})$$

and

$$\mathbf{R}_{ij} = \mathbf{R}_i - \mathbf{R}_j$$

The exchange interaction $J(\mathbf{R}_{ij})$ is not restricted to the nearest neighbors. We now use the Fourier transformations of the exchange interaction and spin;

$$J(\mathbf{q}) = \sum_{j(\neq i)} J(\mathbf{R}_{ij}) \exp(-i\mathbf{q} \cdot \mathbf{R}_{ij}), \tag{2}$$

$$\mathbf{S}_i = \frac{1}{\sqrt{N}} \sum_{\mathbf{q}} \mathbf{S}_{\mathbf{q}} \exp(iq \cdot \mathbf{R}_i) \tag{3}$$

with

$$\mathbf{S}_{\mathbf{q}} = \frac{1}{\sqrt{N}} \sum_i \mathbf{S}_i \exp(-i\mathbf{q} \cdot \mathbf{R}_i)$$

where N $(= N_1 N_2 N_3)$ is the total number of spins, and $S_q^* = S_{-q}$. The position vector $\mathbf{R}_i$ is expressed by

$$\mathbf{R}_i = n_1 \mathbf{a}_1 + n_2 \mathbf{a}_2 + n_3 \mathbf{a}_3 \ (n_1, n_2, n_3 \text{ are integers})$$

where $n_1 = 0 - N_1$, $n_2 = 0 - N_2$, $n_3 = 0 - N_3$, and $\mathbf{a}_1$, $\mathbf{a}_2$, and $\mathbf{a}_3$ are the fundamental lattice vectors. We also define the reciprocal lattice vector G by

$$G(h, k, l) = h\mathbf{b}_1 + k\mathbf{b}_2 + l\mathbf{b}_3 \ (h, k, l \text{ are integers})$$

where $\mathbf{b}_1$, $\mathbf{b}_2$, and $\mathbf{b}_3$ are fundamental reciprocal lattice vectors and are given by

$$\mathbf{b}_1 = 2\pi \frac{\mathbf{a}_2 \times \mathbf{a}_3}{[\mathbf{a}_1, \mathbf{a}_2, \mathbf{a}_3]}, \mathbf{b}_2 = 2\pi \frac{\mathbf{a}_3 \times \mathbf{a}_1}{[\mathbf{a}_1, \mathbf{a}_2, \mathbf{a}_3]}, \mathbf{b}_3 = 2\pi \frac{\mathbf{a}_1 \times \mathbf{a}_2}{[\mathbf{a}_1, \mathbf{a}_2, \mathbf{a}_3]}$$

with

$$[\mathbf{a}_1, \mathbf{a}_2, \mathbf{a}_3] = \mathbf{a}_1 \cdot (\mathbf{a}_2 \times \mathbf{a}_3) = \mathbf{a}_2 \cdot (\mathbf{a}_3 \times \mathbf{a}_1) = \mathbf{a}_3 \cdot (\mathbf{a}_1 \times \mathbf{a}_2).$$

Noting that

$$\mathbf{a}_1 \cdot \mathbf{b}_1 = 2\pi, \mathbf{a}_2 \cdot \mathbf{b}_2 = 2\pi, \mathbf{a}_3 \cdot \mathbf{b}_3 = 2\pi,$$

we have

$$\mathbf{G}(h, k, l) \cdot \mathbf{R}_i = 2\pi(n_1 h + n_2 k + n_3 l) = 2\pi \times \text{integer}.$$

The periodic boundary condition for $\mathbf{S}_i$ leads to

$$\exp[i\mathbf{q} \cdot (N_1 \mathbf{a}_1)] = 1, \exp[i\mathbf{q} \cdot (N_2 \mathbf{a}_2)] = 1, \exp[i\mathbf{q} \cdot (N_3 \mathbf{a}_3)] = 1.$$

This means that the wavevector $\mathbf{q}$ is given by

$$\mathbf{q} = q_1 \mathbf{b}_1 + q_2 \mathbf{b}_2 + q_3 \mathbf{b}_3,$$

where

$$q_1 = \frac{m_1}{N_1}, q_2 = \frac{m_2}{N_2}, q_3 = \frac{m_3}{N_2}.$$

For convenience we assume that

$$-\frac{N_1}{2} \leq m_1 \leq \frac{N_1}{2}, -\frac{N_2}{2} \leq m_2 \leq \frac{N_2}{2}, -\frac{N_3}{2} \leq m_3 \leq \frac{N_3}{2}$$

corresponding to the first Brillouin zone. There are $N_1 N_2 N_3 = N$ wavevectors in the first Brillouin zone. The spin Hamiltonian is rewritten as

$$H = -\sum_{\mathbf{q}} J(\mathbf{q}) \mathbf{S}_{\mathbf{q}} \cdot \mathbf{S}_{-\mathbf{q}}. \tag{4}$$

We look for the lowest minimum of Eq.(1) under the condition that

$$\mathbf{S}_i^2 = S^2 = \frac{1}{N} \sum_{\mathbf{q},\mathbf{q}'} \mathbf{S}_{\mathbf{q}} \cdot \mathbf{S}_{-\mathbf{q}'} \exp[i(\mathbf{q} - \mathbf{q}') \cdot \mathbf{R}_i], \tag{5}$$

for any i. Instead of this condition, we impose a milder condition

$$NS^2 = \sum_i \mathbf{S}_i^2 = \frac{1}{N} \sum_i \sum_{\mathbf{q},\mathbf{q}'} \mathbf{S}_{\mathbf{q}} \cdot \mathbf{S}_{-\mathbf{q}'} \exp[i(\mathbf{q} - \mathbf{q}') \cdot R_i]$$

$$= \sum_{\mathbf{q}} \mathbf{S}_{\mathbf{q}} \cdot \mathbf{S}_{-\mathbf{q}} \tag{6}$$

where we use

$$\sum_i \exp[i(\mathbf{q} - \mathbf{q}') \cdot \mathbf{R}_i] = N\delta_{\mathbf{q},\mathbf{q}'}$$

Under this milder condition, the minimum of Eq.(1) is obtained simply by taking only that $\mathbf{q}$ for which $J(\mathbf{q})$has

the maximum. Denoting this $\mathbf{q}$ by $\mathbf{Q}$ ($\mathbf{q} = -\mathbf{Q}$ being equally allowed), we have the minimum value of Eq.(4) as

$$-J(\mathbf{Q})(\mathbf{S_Q} \cdot \mathbf{S_{-Q}} + \mathbf{S_{-Q}} \cdot \mathbf{S_Q}).$$

We also obtain

$$\mathbf{S}_i = \frac{1}{\sqrt{N}}[\mathbf{S_Q}\exp(i\mathbf{Q}\cdot\mathbf{R}_i) + \mathbf{S_{-Q}}\exp(-i\mathbf{Q}\cdot\mathbf{R}_i)]$$

The condition (6) can be written as

$$\begin{aligned}NS^2 &= 2\mathbf{S_Q}\cdot\mathbf{S_{-Q}} + \mathbf{S_Q}\cdot\mathbf{S_Q}\exp[2i\mathbf{Q}\cdot\mathbf{R}_i]\\ &+ \mathbf{S_{-Q}}\cdot\mathbf{S_{-Q}}\exp[-2i\mathbf{Q}\cdot\mathbf{R}_i],\end{aligned}$$

for any $\mathbf{R}_i$. This indicates that

$$\mathbf{S_Q} \cdot \mathbf{S_Q} = 0. \qquad (7)$$

Here we assume that

$$\begin{aligned}\mathbf{S_Q} &= \mathbf{R_Q} + iI_\mathbf{Q},\\ \mathbf{S_{-Q}} &= \mathbf{R_Q} - iI_\mathbf{Q},\end{aligned}$$

where $\mathbf{R_Q}$ and $\mathbf{I}_Q$ are real vectors.

$$\begin{aligned}\mathbf{S_Q}\cdot\mathbf{S_{-Q}} &= (\mathbf{R_Q} + i\mathbf{I_Q})\cdot(\mathbf{R_Q} - i\mathbf{I_Q})\\ &= \mathbf{R_Q}\cdot\mathbf{R_Q} + \mathbf{I_Q}\cdot\mathbf{I_Q}\\ \mathbf{S_Q}\cdot\mathbf{S_Q} &= (\mathbf{R_Q} + i\mathbf{I_Q})\cdot(\mathbf{R_Q} + i\mathbf{I_Q})\\ &= \mathbf{R_Q}\cdot\mathbf{R_Q} - \mathbf{I_Q}\cdot I_\mathbf{Q} + 2iR_\mathbf{Q}\cdot\mathbf{I_Q} = 0. (8)\end{aligned}$$

Then we have

$$\begin{aligned}R_\mathbf{Q} &= I_\mathbf{Q}\\ \mathbf{R_Q}\cdot\mathbf{I_Q} &= 0.\end{aligned}$$

Then the vector $\mathbf{R_Q}$ is perpendicular to the vector $\mathbf{I_Q}$, and the magnitude $R_\mathbf{Q}$ is the same as the magnitude $I_\mathbf{Q}$. From Eq.(8), we get

$$R_\mathbf{Q}^2 = I_\mathbf{Q}^2 = \frac{1}{4}NS^2.$$

The minimum energy E_{min} is obtained as

$$E_{min} = -NS^2 J(\mathbf{Q}). \qquad (9)$$

The spin vector is expressed by

$$\begin{aligned}\mathbf{S}_i &= \frac{1}{\sqrt{N}}[(\mathbf{R_Q} + i\mathbf{I_Q})\exp(i\mathbf{Q}\cdot\mathbf{R}_i)\\ &+ (\mathbf{R_Q} - i\mathbf{I_Q})\exp(-i\mathbf{Q}\cdot\mathbf{R}_i)]\\ &= \frac{2}{\sqrt{N}}[(\mathbf{R_Q}\cos(\mathbf{Q}\cdot\mathbf{R}_i) - I_\mathbf{Q}\sin(\mathbf{Q}\cdot\mathbf{R}_i)]\\ &= S[(\hat{\mathbf{R}}_\mathbf{Q}\cos(\mathbf{Q}\cdot\mathbf{R}_i) - \hat{\mathbf{I}}_\mathbf{Q}\sin(\mathbf{Q}\cdot\mathbf{R}_i)]\end{aligned}$$

where $\hat{\mathbf{R}}_\mathbf{Q}$ and $\hat{\mathbf{I}}_\mathbf{Q}$ are the unit vectors which are perpendicular to each other. For convenience, $\hat{\mathbf{R}}_\mathbf{Q}$ and $\hat{\mathbf{I}}_\mathbf{Q}$ are in the x-y plane. The z axis is perpendicular to the x-y

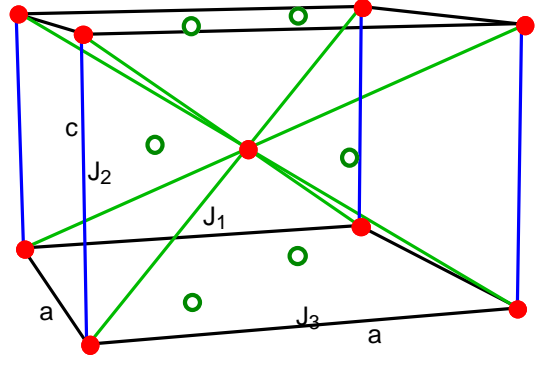FIG. 1: (Color online) The position of Mn^{4+} ions (denoted by solid circles) and O^{2-} (denoted by open circles) in β-MnO$_2$ (rutile-type structure, space group P4$_2$/mmm). $a = b = 4.396\mathring{A}$. $c = 2.871\mathring{A}$. J_1, J_2, and J_3 are the exchange interactions between Mn^{2+} spins. One of the O atom is located at (ua, ua), where $u = 0.302$.

plane. Then using the unit vectors $\mathbf{e}_x$ and $\mathbf{e}_y$, we get the final result

$$\mathbf{S}_i = S[\cos(\mathbf{Q}\cdot\mathbf{R}_i + \phi)\mathbf{e}_x + \sin(\mathbf{Q}\cdot\mathbf{R}_i + \phi)\mathbf{e}_y], \quad (10)$$

where ϕ is the angle between $\hat{\mathbf{R}}_\mathbf{Q}$ and x axis.

The spin structure thus derived is the most fundamental spin structure and is realized as a result of the minimum energy state in the classical spin system. The ferromagnetic state ($\mathbf{Q} = 0$) and antiferromagnetic state ($\mathbf{Q}$ = the zone boundary of the first Brillouin zone) are the special case of the spin structures. In general, $\mathbf{Q}$ is not related to the crystal structure, but is related to the details of the exchange interactions.

III. HELICAL SPIN ORDER FOR β-MnO$_2$

A. Calculation of $J(\mathbf{q})$ for β-MnO$_2$

Figure 1 shows the structure (rutile) of β-MnO$_2$ where $a = b = 4.396\mathring{A}$, $c = 2.871\mathring{A}$, and $u = 0.302$.[8] The exchange interactions J_1, J_2, and J_3 defined by Fig. 1 are antiferromagnetic. The definition of J_1, J_2, and J_3 are the same as that used by Yoshimori. The Néel temperature T_N is equal to 92 K. Each Mn^{4+} ion and surrounding six O^{2-} ions form a cation-occupied deformed octahedron (we will discuss later).

Here we calculate $J(\mathbf{q})$ for MnO$_2$, where the wavenumber $\mathbf{q}$, the lattice vectors $\mathbf{a}(n)$ ($n = 1, 2,\ldots, 4$) and $\mathbf{c}$ are given by

$$\begin{aligned}\mathbf{q} &= (q_x, q_y, q_z),\\ \mathbf{a}(n) &= a\cos[\frac{\pi}{2}(n-1)], a\sin[\frac{\pi}{2}(n-1)], 0,\\ \mathbf{c} &= (0, 0, c).\end{aligned}$$

Then the expression of $J(\mathbf{q})$ is given by

$$
\begin{aligned}
J(\mathbf{q}) \;=\; & J_1 \exp[i\mathbf{q}\cdot \frac{\mathbf{c}+\mathbf{a}(1)+\mathbf{a}(2)}{2}] + J_1 \exp[i\mathbf{q}\cdot \frac{-\mathbf{c}+\mathbf{a}(1)+\mathbf{a}(2)}{2}] \\
& + J_1 \exp[i\mathbf{q}\cdot \frac{\mathbf{c}+\mathbf{a}(2)+\mathbf{a}(3)}{2}] + J_1 \exp[i\mathbf{q}\cdot \frac{-\mathbf{c}+\mathbf{a}(2)+\mathbf{a}(3)}{2}] \\
& + J_1 \exp[i\mathbf{q}\cdot \frac{\mathbf{c}+\mathbf{a}(3)+\mathbf{a}(4)}{2}] + J_1 \exp[i\mathbf{q}\cdot \frac{-\mathbf{c}+\mathbf{a}(3)+\mathbf{a}(4)}{2}] \\
& + J_1 \exp[i\mathbf{q}\cdot \frac{\mathbf{c}+\mathbf{a}(4)+\mathbf{a}(1)}{2}] + J_1 \exp[i\mathbf{q}\cdot \frac{-\mathbf{c}+\mathbf{a}(4)+\mathbf{a}(1)}{2}] \\
& + J_2 \exp[i\mathbf{q}\cdot \mathbf{c}] + J_2 \exp[-i\mathbf{q}\cdot \mathbf{c}] \\
& + J_3 \exp[i\mathbf{q}\cdot \mathbf{a}(1)] + J_3 \exp[-i\mathbf{q}\cdot \mathbf{a}(1)] + J_3 \exp[i\mathbf{q}\cdot \mathbf{a}(2)] + J_3 \exp[-i\mathbf{q}\cdot \mathbf{a}(2)].
\end{aligned} \tag{11}
$$

Then $J(\mathbf{q})$ can be rewritten as

$$
\begin{aligned}
J(\mathbf{q}) \;=\; & J(h,k,l) = 8J_1 \cos(\pi h)\cos(\pi k)\cos(\pi l) \\
& + 2J_2 \cos(2\pi l) + 2J_3[\cos(2\pi h) + \cos(2\pi k)] \tag{12}
\end{aligned}
$$

where

$$
q_x = (\frac{2\pi}{a})h = a^*h, \quad q_y = (\frac{2\pi}{a})k = a^*k, \quad q_z = (\frac{2\pi}{c})l = c^*l
$$

with h, k, and l being dimensionless numbers and a^* and c^* are reciprocal lattice constants.

B. Mathematica programs used in the present work

In order to determine the magnetic Bragg peaks in the reciprocal lattice plane, we use the following three Mathematica programs, ContourPlot for the equi-energy contour plot, FindMaximum for finding maximum, and ListVectorPlot3D for drawing the spin directions in the lattice points of the real space.

1. Contour plot program

This program is used to determine the overview on the positions of the magnetic Bragg peaks in the (h,k,l) reciprocal lattice plane, where one of h, k, and l are fixed. When the values of J_1, J_2, and J_3 are given, using the Mathematica program [ContourPlot], we can make a plot of the contours of $J(h,k,l) = a$ (constant) in the (h,k,l) plane, where the parameter a is changed appropriately such that the maximum value of $J(h,k,l)$ is obtained. This program is very useful to find the selection rule for the position of the magnetic Bragg peaks, as a function of J_1, J_2, and J_3.

2. Finding maximum program

This program is used to determine the exact position of the magnetic Bragg peak in the (h,k,l) reciprocal lattice

plane, where one of h, k, and l are fixed. For convenience, here we assume that l is fixed such that $l = 0$. Using the Mathematica program [FindMaximum], we find the maximum value of $J(h,k,l)$ for given J_2 and J_3, where J_1 (= -1) is fixed, and the regions of h and k are appropriately chosen. This program is very convenient when one wants to know how the position of the Bragg point changes as a function of J_2 and J_3.

3. ListVectorPlot3D program

This program is used to draw the spin directions at each lattice sites in the real space. The spin structure depends on the values of $\mathbf{Q}$.

IV. SELECTION RULE FOR THE MAGNETIC BRAGG PEAKS FROM SIMPLE ANALYSIS

A. Distribution of magnetic Bragg peaks in the (h, k, l = fixed integer) reciprocal lattice plane

The magnetic Bragg peaks can be located at the wavevector $\mathbf{q}$, where $J(h,k,l)$ takes a maximum. When l = fixed integer, $J(h,k,l)$ is given by

$$
\begin{aligned}
J(h,k,l) \;=\; & 8J_1(-1)^l \cos(\pi h)\cos(\pi k) \\
& + 2J_2 + 2J_3[\cos(2\pi h) + \cos(2\pi k)],
\end{aligned}
$$

suggesting that the location of the magnetic Bragg peaks in the (h, k, l = fixed integer) reciprocal lattice plane depends only on J_1 and J_3,and is independent of the J_2. The selection rule can be derived as follows.
(i) The distribution of the magnetic Bragg peaks is the same in the reciprocal lattice planes, $(h, k, 1)$, $(h, k, 3)$, $(h, k, 5)$, $(h, k, 7)$,...
(ii) The distribution of the magnetic Bragg peaks is the same in the reciprocal lattice planes , $(h, k, 0)$, $(h, k, 2)$, $(h, k, 4)$, $(h, k, 8)$,...

B. Magnetic Bragg peaks along the l direction with $h =$ fixed integer and $k = 0$

When $k = 0$ and h is a fixed integer, $J(h =$ fixed integer, $k = 0, l)$ is rewritten as

$$J(h, 0, l) = 8(-1)^h J_1 \cos(\pi l) + 2J_2 \cos(2\pi l) + 2J_3,$$

which indicates that the location of the magnetic Bragg peaks along the ($h =$ fixed integer, $k = 0$, l) direction depends only on J_1 and J_2, and is independent of J_3. The following selection rules can be derived.
(i) The location of the magnetic Bragg peaks along the l direction is the same for $(1, 0, l)$, $(3, 0, l)$, $(5, 0, l)$, $(7, 0, l)$, $\cdots$.
(ii) The location of the magnetic Bragg peaks along the l direction is the same for $(0, 0, l)$, $(2, 0, l)$, $(4, 0, l)$, $(8, 0, l)$, $\cdots$.

C. Magnetic Bragg peaks along the l direction with $h = k =$ half inetgers

For $h = k =$ half-integer $(= 1/2, 3/2, 5/2, \cdots)$, we have

$$J(h, h, l) = 2J_2 \cos(2\pi l) - 4J_3,$$

leading to the appearance of the magnetic Bragg peaks appear at

$$l = 1/2, 3/2, 5/2, \cdots$$

for $h = k = 1/2, 3/2, 5/2, 7/2, \cdots$.

D. Magnetic Bragg peaks along the (0, 0,l) direction

For any l, $J(0,0,l)$ can be expressed by

$$J(h = 0, k = 0, l) = J(\theta) = 8J_1 \cos(\theta) + 2J_2 \cos(2\theta) + 4J_3.$$

with $\theta = \pi l$. This indicates that the location of the magnetic Bragg peaks along the $(0,0,l)$ direction, is independent of J_3. The derivative of $J(0,0,l)$ with respect to θ is obtained as

$$\frac{dJ(\theta)}{d\theta} = -4[J_1 + J_2 \cos(\theta)] \sin(\theta) = 0.$$

Then we get the two solutions.
(i) Ferromagnetic or antiferromagnetic configurations

$$\sin\theta = 0, \ \theta = 0, \pi.$$

where

$$J(\theta = 0) = 8J_1 + 2J_2 + 4J_3$$
$$J(\theta = \pi) = -8J_1 + 2J_2 + 4J_3.$$

(ii) Helical spin configuration

$$\cos\theta = -J_1/J_2, \theta = \theta_0 = \arccos(-J_1/J_2),$$

under the condition of $|J_1/J_2| < 1$, where

$$J(\theta = \theta_0) = -4\frac{J_1^2}{J_2} - 2J_2 + 4J_3.$$

The difference is calculated as

$$J(\theta = \theta_0) - J(\theta = \pi) = -4J_2(\frac{J_1}{J_2} - 1)^2,$$
$$J(\theta = \theta_0) - J(\theta = 0) = -4J_2(\frac{J_1}{J_2} + 1)^2.$$

Then the helical spin order appears when

$$J(\theta = \theta_0) > J(\theta = \pi),$$
$$J(\theta = \theta_0) > J(\theta = \pi).$$

If the conditions $J_2 < 0$ and $|J_1/J_2| < 1$ are satisfied, the magnetic Bragg peaks appear at the wavevectors denoted by

$$(h, k, l) = (0, 0, 1\pm\epsilon), (0, 0, 3\pm\epsilon), (0, 0, 5\pm\epsilon), (0, 0, 7\pm\epsilon), \cdots,$$

where ϵ is defined as

$$\cos(\pi\epsilon) = \frac{J_1}{J_2}.$$

E. Magnetic Bragg peaks along the $(h, 0, 0)$ direction

$J(h, k = 0, l = 0)$ and its derivative are given by

$$J(h, k = 0, l = 0) = 8J_1 \cos(\pi h) + 2J_3 \cos(2\pi h) + 2J_2 + 2J_3,$$

and

$$\frac{dJ(h, k = 0, l = 0)}{dh} = 8\pi[J_1 - J_3 \cos(\pi h)] \sin(\pi h),$$

respectively. Since $|J_1/J_3| > 1$ in MnO_2, we have only $\sin(\pi h) = 0$. Since $J_1 < 0$, we have the following selection rule. The magnetic Bragg appears only at

$$(1, 0, 0), (3, 0, 0), (5, 0, 0), (7, 0, 0), \cdots$$

along the h-direction.

V. DETERMINATION OF J_2 AND J_3 FROM EXPERIMENTAL DATA ON β-MnO$_2$

A. The ratio J_2/J_1

We now calculate the value of ϵ, at which $J(h = 1, k = 0, l = 2 + \epsilon)$ takes a maximum, as a function of J_2, where $J_1 = -1$. The value of ϵ is uniquely determined as a
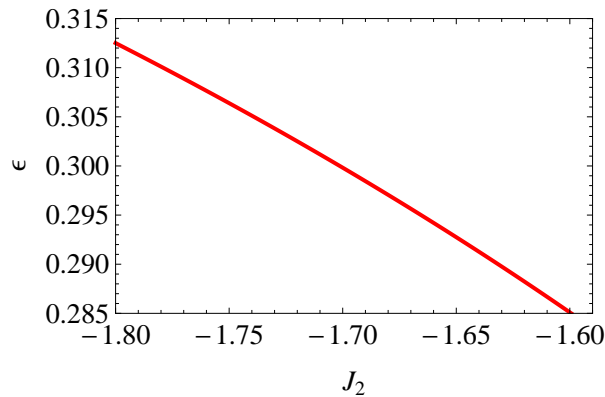
FIG. 2: (Color online) Plot of ϵ as a function of J_2. $J_1 = -1$

FIG. 3: (Color online) Plot of $|\Theta|/T_N$ as a function of p_3, where $p_2 = 1.68469$.

function J_2 as shown in Fig. 2. When $J_2 = -1.6039$, we find $\epsilon = 2/7$ (Yoshimori[1]).

Experimentally, the magnetic Bragg peak is observed at $(h = 1, k = 0, l = 2.29771)$ for β-MnO$_2$. Here we note that $l = 2.29771 = 2 + 2/7 + 0.0120$. The value of l is slightly deviated from the value of $2 + 2/7$, which is predicted by Yoshimori.[1] $J(h = 1, k = 0, l)$ and its derivative are given by

$$J(h = 1, k = 0, l) = -8J_1 \cos(\pi l) + 2J_2 \cos(2\pi l) + 4J_3,$$

and

$$\frac{J(h = 1, k = 0, l)}{dl} = 4\pi[2J_1 \sin(\pi l) - J_2 \sin(2\pi l)],$$

respectively. $J(h = 1, k = 0, l)$ has a maximum when

$$\cos(\pi l) = \frac{J_1}{J_2}.$$

or

$$l = 1 \pm \epsilon, 3 \pm \epsilon, 5 \pm \epsilon, \cdots,$$

where

$$\cos(\pi \epsilon) = \frac{J_1}{J_2}.$$

Note that $J(h = 0, k = 0, l)$ has a maximum when

$$\cos(\pi l) = -\frac{J_1}{J_2}.$$

Since the magnetic Bragg peak appears at $l = 2.29771$, we have

$$\frac{J_1}{J_2} = 0.59359$$

or

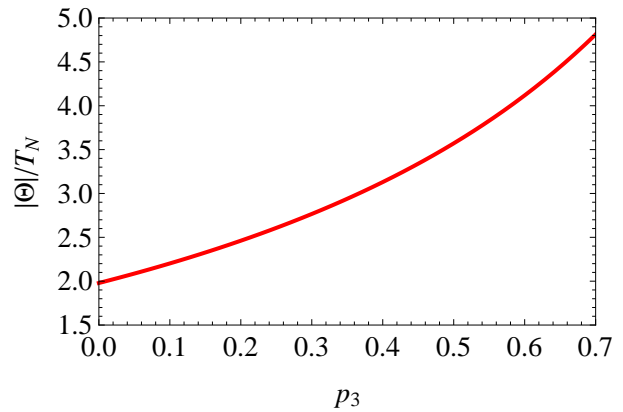$$\frac{J_2}{J_1} = 1.68469$$

indicating that $J_2 < 0$ since $J_1 < 0$.

B. Ratio $p_3 = J_3/J_1$

The ratio J_3/J_1 cannot be determined uniquely from the experimental results on the magnetic neutron scattering or x-ray magnetic scattering. The ratio $|\Theta|/T_N$ can be calculated as

$$\frac{|\Theta|}{T_N} = \frac{J(0)}{J(\theta_0)} = \frac{4 + p_2 + 2p_3}{\frac{2}{p_2} + p_2 - 2p_3}, \quad (13)$$

where $p_2 = J_2/J_1$, $p_3 = J_3/J_1$, Θ is the Curie-Weiss temperature (the value is negative for β-MnO$_2$) and T_N is the Néel temperature. The value of p_3 can be determined from the ratio $|\Theta|/T_N$ since p_2 is already determined. We make a plot of $|\Theta|/T_N$ as a function of p_3 in Fig. 3.

As far as we know, there have been several reports on the experimental values of Θ and T_N for β-MnO$_2$; $\Theta = -316$ K, $T_N = 84$ K [Bizette and B. Tsai (1949)],[10] $\Theta = -1050$ K, $T_N = 92$ K [Ohama and Hamaguchi (1971)],[12] $\Theta = -783$ K, $T_N = 92$ K [Sato et al.(2000)],[8] respectively. Using the values of T_N, Θ and the value of p_2 $(= 1.68469)$ determined above, the value of p_3 can be calculated as $p_3 = 0.537, 0.986, 1.091$ using the data of Bizette and Tsai,[10] Sato et al.,[8] and Ohama and Hamaguchi,[3] respectively.

We note that the boundary of the helical phase is described by (the derivation will be shown later)

$$p_3 = 1/p_2 \text{ or } J_2 J_3 = J_1^2. \quad (14)$$

The helical order can exist when $p_3 < 1/p_2$. When $p_2 = 1.68469$ for MnO$_2$, p_3 should be lower than 0.5935. In other words, the ratio $|\Theta|/T_N$ should be lower than 4.07853. Since $T_N = 92$ K, this means that $|\Theta|$ should be smaller than 375.2 K. The value of $|\Theta|$ by Bizette and Tsai seems to be reasonable, while the values of $|\Theta|$ obtained by Sato et al.[8] and Ohama and Hamaguchi[3] are much higher than 375.2 K. Note that Yoshimori[1] predicts that the boundary is described by $p_3 p_2 = 1/2$. This expression is not correct according to our calculation.
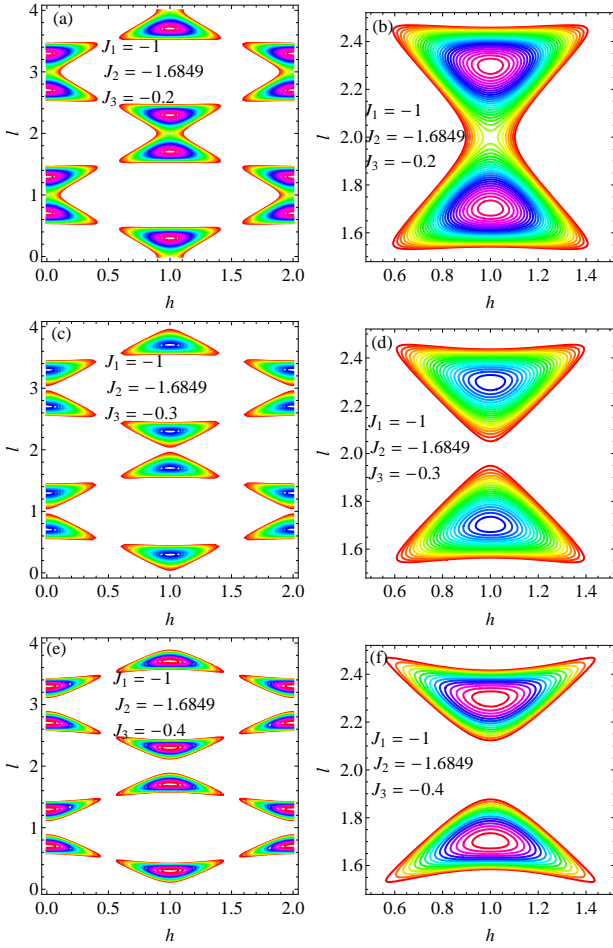
FIG. 4: (Color online) (a)(b) Distribution of magnetic Bragg points in the $(h, k = 0, l)$ reciprocal lattice plane. $J_1 = -1$, $J_2 = -1.68469$. $J_3 = -0.2$. $p_3 = J_3/J_1 = 0.2$. (c)(d) Distribution of magnetic Bragg points in the $(h, k = 0, l)$ reciprocal lattice plane. $J_1 = -1$, $J_2 = -1.68469$. $J_3 = -0.3$. $p_3 = J_3/J_1 = 0.3$. (e)(f) Distribution of magnetic Bragg points in the $(h, k = 0, l)$ reciprocal plane around $h = 1$ and $l = 2$. $J_1 = -1$, $J_2 = -1.68469$. $J_3 = -0.4$. $p_3 = J_3/J_1 = 0.4$.

VI. NUMERICAL CALCULATION

A. The contour plot of $J(h, 0, l)$ in the $(h, 0, l)$ reciprocal lattice plane

Using the numerical calculation of the contour plot using the Mathematica, we find the location of the magnetic Bragg peaks in the $(h, 0, l)$ reciprocal lattice, where

$$J(h, 0, l) = 8J_1 \cos(\pi h) \cos(\pi l) + 2J_2 \cos(2\pi l) + 2J_3[\cos(2\pi h) + 1],$$

takes a maximum, where $J_1 = -1$, $J_2 = p_2 J_1 = -1.68469$, and $J_3 = p_3 J_1 = -0.3$. Figures 4(a)-(f) show the contour plot of $J(h, 0, l)$ in the reciprocal lattice plane of $(h, 0, l)$, where p_3 is changed as a parameter $(p_3 < 0.5935)$. As is predicted above, we find that the magnetic Bragg peaks appear at

$$(0, 0, 1 \pm \epsilon), (0, 0, 3 \pm \epsilon), (0, 0, 5 \pm \epsilon), (0, 0, 7 \pm \epsilon), \ldots,$$
$$(1, 0, 0 \pm \epsilon), (1, 0, 2 \pm \epsilon), (1, 0, 4 \pm \epsilon), (1, 0, 6 \pm \epsilon), \ldots,$$
$$(2, 0, 1 \pm \epsilon), (2, 0, 3 \pm \epsilon), (2, 0, 5 \pm \epsilon), (2, 0, 7 \pm \epsilon), \ldots,$$

where $\epsilon = 0.29771$ and is independent of p_3 $(p_3 < 0.5935)$. Note that the essential results are independent of the choice of p_3 at least for $0.2 \le p_3 \le 0.4$.

B. The contour plot of $J(h, k = h, l)$ in the $(h, k = h, l)$ reciprocal lattice plane

Using the contour plot of the $J(h, k = h, l)$, we find the location of the magnetic Braggs in the (h, h, l) reciprocal lattice, where

$$J(h, h, l) = 8J_1 \cos^2(\pi h) \cos(\pi l) + 2J_2 \cos(2\pi l) + 4J_3 \cos(2\pi h).$$

The location of the magnetic Bragg peaks is given by

$$(0, 0, 1 \pm \epsilon), (0, 0, 3 \pm \epsilon), (0, 0, 5 \pm \epsilon), (0, 0, 7 \pm \epsilon), \ldots,$$
$$(1/2, 1/2, 1/2), (1/2, 1/2, 3/2), (1/2, 1/2, 5/2), (1/2, 1/2, 7/2), \ldots,$$
$$(1, 1, 1 \pm \epsilon), (1, 1, 3 \pm \epsilon), (1, 1, 5 \pm \epsilon), (1, 1, 7 \pm \epsilon), \ldots,$$
$$(3/2, 3/2, 1/2)(3/2, 3/2, 3/2), (3/2, 3/2, 5/2), (3/2, 3/2, 7/2), \ldots,$$

in the reciprocal lattice plane of $(h, k = h, l)$, where $\epsilon = 0.29771$.

C. The contour plot in the (h, k, l) plane with $l = 2n$

Using the contour plot of the Mathematica, we find the location of the magnetic Braggs in the $(h, k, l = 2n)$
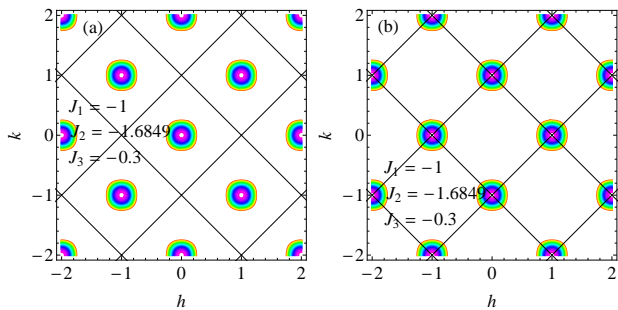
FIG. 5: (Color online) (a) Magnetic Bragg points in the $(h, k, l = 2n)$ reciprocal lattice plane. (b) Magnetic Bragg points in the $(h, k, l = 2n + 1)$ reciprocal lattice plane. $J_1 = -1$, $J_2 = -1.68469$. $J_3 = -0.3$. $p_3 = 0.3$.

reciprocal lattice, where

$$J(h, k, l = 2n) = 8J_1 \cos(\pi h) \cos(\pi k) \\ + 2J_3[\cos(2\pi h) + \cos(2\pi k)] + 2J_2,$$

which does not depend on the index n. Figures 5(a) show the location of magnetic Bragg peaks in the in-plane $(h, k, l = 2n)$ reciprocal lattice plane. We find that the magnetic Bragg peaks appear for $h + k =$ odd. This selection rule is true for $l = 2n$ with any integer n.

D. The contour plot in the (h, k, l) plane with $l = 2n + 1$

Using the contour plot of the Mathematica, we find the location of the magnetic Braggs in the $(h, k, l = 2n + 1)$ reciprocal lattice, where

$$J(h, k, l = 2n + 1) = -8J_1 \cos(\pi h) \cos(\pi k)) \\ + 2J_3[\cos(2\pi h) + \cos(2\pi k)] + 2J_2,$$

which does not depend on the index n. Figure 5(b) show the location of the magnetic Bragg peaks in the in-plane $(h, k, l = 2n + 1)$ reciprocal lattice plane, where n is the integer. The magnetic Bragg peaks appear for $h + k =$ even for $l = 2n + 1$.

VII. PHASE DIAGRAM IN THE (J_2, J_3) PLANE

The phase diagram for $J_1 = -1$ can be determined using the programs of the ContourPlot and FindMaximum. The phase diagram consists of the four phases; (i) the helical order along the c axis, (ii) the helical order along the a axis, (iii) the ordered phase with $h = 1/2$, $k = 0$, and $l = 1/2$, and (iv) the ordered phase with $h = 0$, $k = 0$, $l = 1$.

A. Ordered phases

1. Helical order along the c axis

Spins in the same ab plane are parallel, i.e., $h = 0$ and $k = 0$. They screw along the c axis. We find the maximum of

$$J(h = 0, k = 0, l) = 4J_3 + 8J_1 \cos(l\pi) \\ + 2J_2 \cos(2l\pi),$$

by taking the derivative of $J(h = 0, k = 0, l)$ with respect to l. The condition of the local maximum is given by

$$\cos(\pi l_{max}) = -\frac{J_1}{J_2},$$

where $|J_1/J_2| < 1$. Then the maximum of $J(h = 0, k = 0, l)$ is given by

$$J_{max}(h = 0, k = 0, l = l_{max}) = 4J_3 - 4\frac{J_1^2}{J_2} - 2J_2$$

for the helical order with ($h = 0$, $k = 0$, and $l = l_{max}$)

$$\cos(\pi l_{max}) = -\frac{J_1}{J_2} = -\frac{1}{1.68468} = -0.59358,$$
$$l_{max} = 0.70228.$$

2. Helical order along the a axis

The helical spin order where the spins in the same bc plane are parallel and they screw along the a axis. We find the maximum of

$$J(h, k = 0, l = 1) = 2J_2 + 2J_3 + 8J_1 \cos(\pi h) + 2J_3 \cos(2\pi h),$$

by taking the derivative of $J(h, k = 0, l = 0)$ with respect to h. The condition of the local maximum is given by

$$\cos(\pi h_{max}) = -\frac{J_1}{J_3},$$

where $|J_1/J_3| < 1$. The maximum value is

$$J_{max}(h_{max}, k = 0, l = 1) = 2J_2 - 4\frac{J_1^2}{J_3}.$$

3. The ordered phase with h = 0, k = 0, and l = 1

$J(h = 0, k = 0, l = 1)$ is given by

$$J(h = 0, k = 0, l = 1) = -8J_1 + 2J_2 + 4J_3.$$

4. The ordered phase with h = 1/2, k = 0, and l = 1/2

This phase corresponds to the MnF_2-type antiferromagnetic structure (named by Yoshimori[1]). $J(h = 1/2, k = 0, l = 1/2)$ is evaluated as

$$J(h = 1/2, k = 0, l = 1/2) = -2J_2.$$

B. Boundaries between ordered phases

1. The phase boundary between the spin order with the phase ($h = 1/2$, $k = 0$, and $l = 1/2$) and the helical spin order along the c axis

The difference of $J(h, k, l)$ between the helical spin order along the c axis and the phase ($h = 1/2, k = 0, l = 1/2$) is given by

$$J_{\max}(h = 0, k = 0, l = l_{\max}) - J(h = 1/2, k = 0, l = 1/2)$$
$$= 4J_2 - 4\frac{J_1^2}{J_3}.$$

So the helical ordered phase is energetically favorable when

$$J_2 > \frac{J_1^2}{J_3},$$

with the condition of $|J_1/J_2| < 1$. When $J_3 < 0$, this inequality can be rewritten as

$$J_2 J_3 < J_1^2,$$

or

$$p_2 p_3 < 1.$$

2. The phase boundary between the spin order with ($h = 0$, $k = 0$, $l = 1$) and the spin order with ($h = 1/2$, $k = 0$, $l = 1/2$)

The difference of $J(h, k, l)$ between the ($h = 0, k = 0, l = 1$) and the phase ($h = 1/2, k = 0, l = 1/2$) is given by

$$J(h = 1/2, k = 0, l = 1/2) - J(h = 0, k = 0, l = 1)$$
$$= -4J_2 - 4J_3 + 8J_1$$

where

$$J(h = 0, k = 0, l = 1) = -8J_1 + 2J_2 + 4J_3,$$

and

$$J(h = 1/2, k = 0, l = 1/2) = -2J_2.$$

When

$$2J_1 > J_2 + J_3,$$

the phase ($h = 1/2, k = 0, l = 1/2$) is energetically favorable. When

$$2J_1 < J_2 + J_3.$$

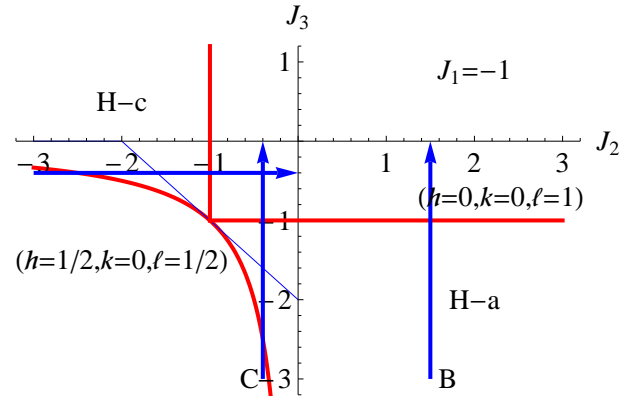the phase $h = 0, k = 0, l = 1$) is energetically favorable.

FIG. 6: (Color online) Scans A, B, and C in the phase diagram (J_2, J_3) to determine the location of the magnetic Bragg peaks in the (h, k, l) reciprocal space. $J_1 = -1$.

3. The phase boundary between the helical order along the a axis and the phase ($h = k = 1/2$, and $l = 1$)

The difference of $J(h, k, l)$ between the ($h = 0, k = 0, l = 1$) and the helical order along the a axis is given by

$$J_{\max}(h_{\max}, k = 0, l = 1) - J(h = 0, k = 0, l = 1)$$
$$= -4J_3(\frac{J_1}{J_3} - 1)^2,$$

where

$$J(h = 0, k = 0, l = 1) = -8J_1 + 2J_2 + 4J_3,$$
$$J_{\max}(h_{\max}, k = 0, l = 1) = 2J_2 - 4\frac{J_1^2}{J_3}.$$

Then the helical order is stable for $J_3 < -1$. This inequality is satisfied for the condition of the helical order

$$|J_1/J_3| < 1.$$

C. Multicritical point ($J_2 = -1$ and $J_3 = -1$ and phase transition lines

All four ordered phases merge only at the multicritical point at ($J_2 = -1$ and $J_3 = -1$), where the line given by $2J_1 = J_2 + J_3$ and the curve $J_2 J_3 = J_1^2$ intersect with other (see the phase diagram of J_3 vs J_2). Note that $J_1 = -1$. As will be shown later, the line ($2J_1 = J_2 + J_3$) is of the first-order. The lines denoted by $J_2 = -1$ and $J_3 = -1$ are of the second-order.
(1) Using the program of finding maximum in $J(\mathbf{q})$ for each point (J_2, J_3) in the phase digram, we find the local maximum point $(h, 0, l)$ in the h-l plane. The location of these points is plotted as a function of J_2 when J_3 is fixed and as a function of J_3 when J_2 is fixed.
(2) Using the program of finding maximum in $J(\mathbf{q})$ for each point (J_2, J_3) in the phase diagram, we find the local
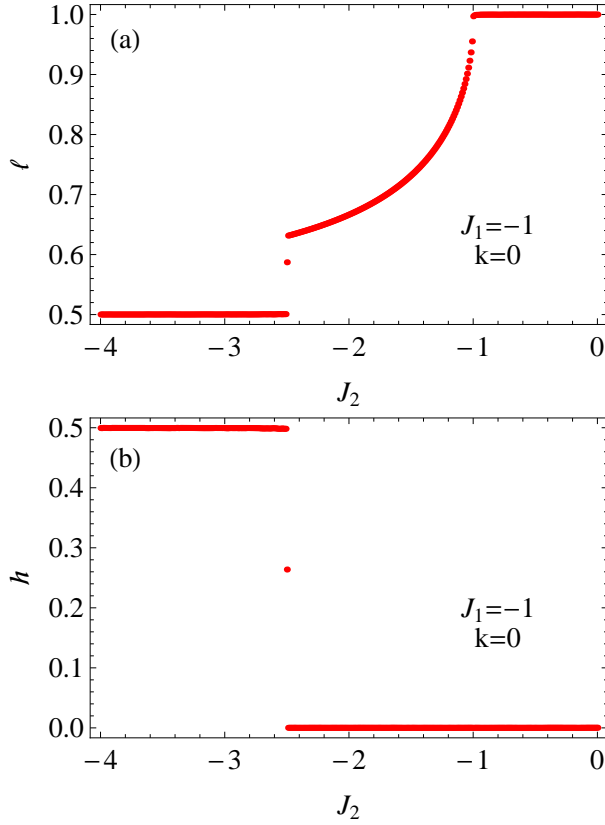
FIG. 7: (Color online) (a) l vs J_2 and (b) h vs J_2 along the scan A ($-4 \leq J_2 \leq 0$ and $J_3 = -0.4$). $k = 0$. $J_1 = -1$.

maximum point $(h, k, 0)$ in the h-k plane These points are plotted as a function of J_2 when J_3 is fixed and as a function of J_3 when J_2 is fixed.

1. Scan A

In the Scan A (see Fig. 6), we choose $J_3 = -0.4$ and $J_1 = -1$. J_2 is changed as a parameter between -4.0 and 0. We make a plot of l vs J_2 in Fig. 7. The discontinuity in l vs J_2 occurs at $J_2 = -2.5$ (the phase boundary between the phase with ($h = 1/2, k = 0, l = 1/2$) and the helical order along the c axis), where the relation $J_2 J_3 = J_1^2$ is satisfied ($J_1 = -1$). We find that the relation of l vs J_2 is well described by

$$\cos(\pi l) = -\frac{J_1}{J_2},$$

for $-2.5 \leq J_2 \leq -1$ (the helical phase along the c axis). The value of l is independent of J_3. For example, when $l = 0.8$, we have $J_2 = -1.24$ as shown in Fig. 7(a). We note that l is equal to 1 at $J_2 = -1$ (the phase boundary between the helical phase along the c axis and the phase with ($h = 0, k = 0, l = 1$) and remain unchanged ($l = 1$) for $-1 \leq J_2 \leq 0$. We also make a plot of h vs J_2 in Fig. 7(b). The value of h undergoes a sudden change
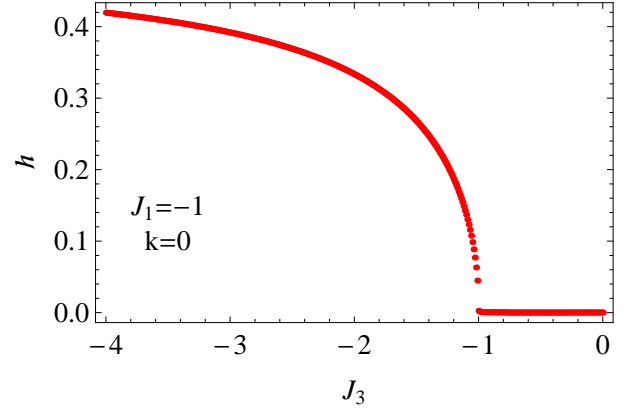

FIG. 8: (Color online) h vs J_3 along the scan B ($-4 \leq J_3 \leq 0$ and $J_2 = 1.5$). $J_1 = -1$. $k = 0$ and $l = 1$.

from $h = 0.5$ to 0 at $J_2 = -2.5$ (at the phase boundary between the phase with ($h = 1/2, k = 0, l = 1/2$) and the helical order along the c axis) and remains constant ($h = 0$) for $-2.5 \leq J_2 \leq 0$. Note that there is no change of h at $J_2 = -1$.

2. Scan B

In the Scan B (see Fig. 6), we choose $J_2 = 1.5$ and $J_1 = -1$. J_3 is changed as a parameter between -4.0 and 0. We make a plot of h vs J_2 in Fig. 8. The value of h decreases with increasing J_3 and reduces to zero at $J_3 = -1$ (the phase boundary (second-order) between the helical order along the a axis and the phase with ($h = 0, k = 0, l = 1$). We find that the relation of h vs J_3 is well described by

$$\cos(\pi h) = -\frac{J_1}{J_3}.$$

The value of h is independent of J_2. For example, when $h = 0.2$, we have $J_3 = -1.236$. The plot of l vs J_2 (which is not shown here) indicates that l remains constant ($l = 1$) for $-4 \leq J_3 \leq 0$, where $J_2 = 1.5$.

3. Scan C

In the Scan C, we choose $J_2 = -0.4$ and $J_1 = -1$. J_3 is changed as a parameter between -3.5 and 0. We make a plot of h vs J_3 and l vs J_3 in Figs. 9(a) and (b). As shown in Fig. 9(a), the value of h decreases with increasing J_3, showing an abrupt decrease at $J_3 = -2.5$ (which is denoted by $J_2 J_3 = J_1^2$) at the phase boundary (first-order) between the phase with ($h = 1/2, k = 0, l = 1/2$) and the helical order along the a axis). The value of h decreases with further increasing J_3, following Eq.(?????), and reduces to zero at $J_3 = -1$ at the phase boundary (second-order) between the helical order along the a axis and the phase with ($h = 0, k = 0, l = 1$).
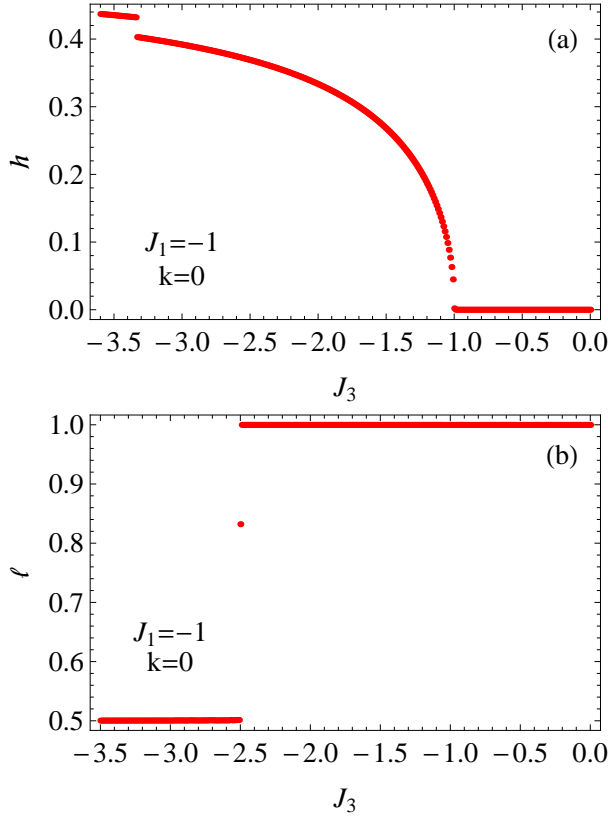
FIG. 9: (Color online) (a) h vs J_3 and (b) l vs J_3 along the scan C ($-3.5 \le J_3 \le 0$ and $J_2 = 0.4$). $J_1 = -1$. $k = 0$.

In Fig. 9(b), the value of l increases with increasing J_3. It shows an abrupt change from $l = 1/2$ to $l = 1$ at $J_3 = -2.5$ at the phase boundary (first-order) between the phase with ($h = 1/2, k = 0, l = 1/2$) and the helical state along the a axis.

VIII.   CONTOUR PLOT OF $(h, 0, l)$ FOR TYPICAL POINTS IN THE (J_2, J_3) PHASE DIAGRAM

Here we show the contour plot of $J(h, 0, l)$ for the typical points in the (J_2, J_3) phase diagram (see Fig. 10). The maximum points in the countour plot of $J(h, 0, l))$ correspond to the magnetic Bragg peaks in the $(h, 0, l)$ plane.

A.   The points A, B, C, D, and E with $J_1 = -1.0$ and $J_2 = -0.5$

Typical contour plot of $(h, 0, l)$ at the points A, B, C, D, and E in the (J_2, J_3) phase diagram are shown in Fig. 11. The point A ($J_3 = -0.5$) is in the phase with ($h = 0, k = 0, l = 1$). The point B ($J_3 = $ -1.5) is in the helical phase with the a axis. The point C ($J_3 = -2$) is the phase boundary between the phase with ($h = 0, k = 0, l = 1$)
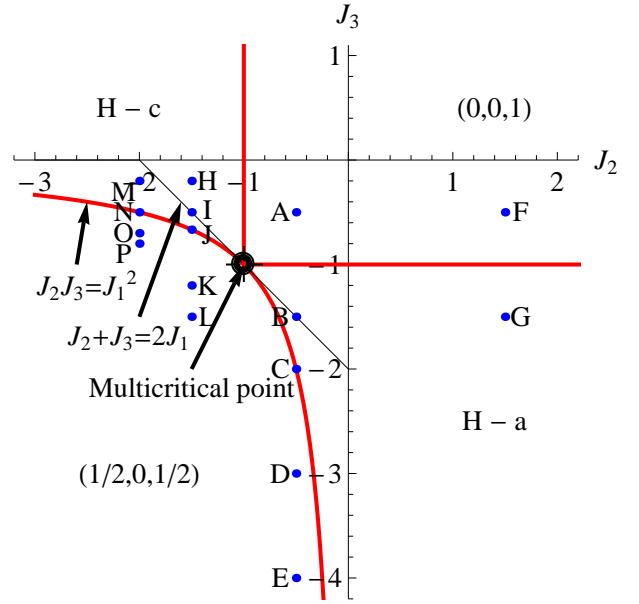

FIG. 10: (Color online) Phase diagram of J_3 vs J_2: $J_1 = -1$. H-a: helical order along the a axis. H-c: helical order along the c axis. The ordered phase with ($h = 1/2, k = 0, l = 1/2$). The ordered phase with ($h = 0, k = 0, l = 1$). The multicritical point is at ($J_2 = -1$, $J_3 = -1$). The calculations of the contour plots are made at the points (A, B, C, $\cdots$, P).

and the helical phase with the a axis. The points D ($J_3 = -3.0$) and E ($J_3 = -4.0$) are in the phase with ($h = 1/2, k = 0, l = 1/2$).

B.   The points F and G with $J_1 = -1.0$ and $J_2 = 1.5$.

Typical contour plot of $(h, 0, l)$ at the points F and G in the (J_2, J_3) phase diagram are shown in Fig. 12. The point F ($J_3 = -0.5$) is in the phase with ($h = 0, k = 0, l = 1$). The point G ($J_3 = -1.5$) is in the helical phase with the a axis.

C.   The points H, I, J, K, and L with $J_1 = -1.0$ and $J_2 = -1.5$

Typical contour plot of $(h, 0, l)$ at the points H, I, J, K, and K in the (J_2, J_3) phase diagram are shown in Fig. 13. The point H ($J_3 = -0.2$) is in the helical phase along the c axis. The point I ($J_3 = -0.5$) is in the helical phase with the c axis and is on the line ($J_2 + J_3 = 2J_1$). The point J ($J_3 = -0.667$) is on the phase boundary between the helical phase with the c axis and the phase with ($h = 1.2, k = 0, l = 1/2$). The points K ($J_3 = -3.0$) and L ($J_3 = -4.0$) are in the phase with ($h = 1/2, k = 0, l = 1/2$).
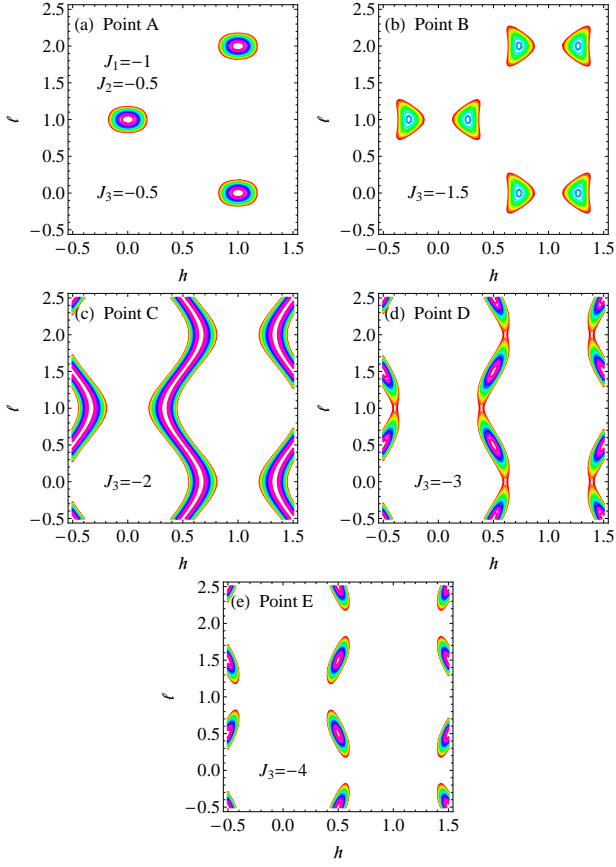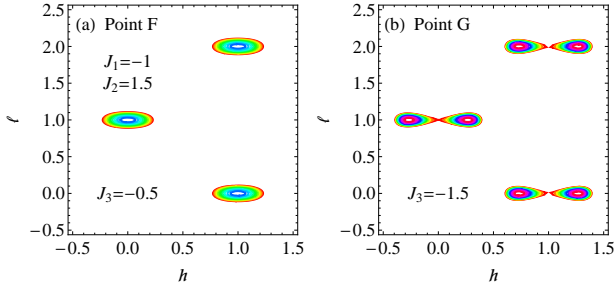
FIG. 11: (Color online) Distribution of Bragg peaks in the $(h, 0, l)$ reciprocal lattice plane. $J_1 = -1$. $J_2 = -0.5$, and J_3 is changed as a parameter. (a) Point A ($J_3 = -0.5$), (b) Point B ($J_3 = -1.5$), (c) Point C ($J_3 = -2.0$), (d) Point D ($J_3 = -3.0$), and (e) Point E ($J_3 = -4.0$).
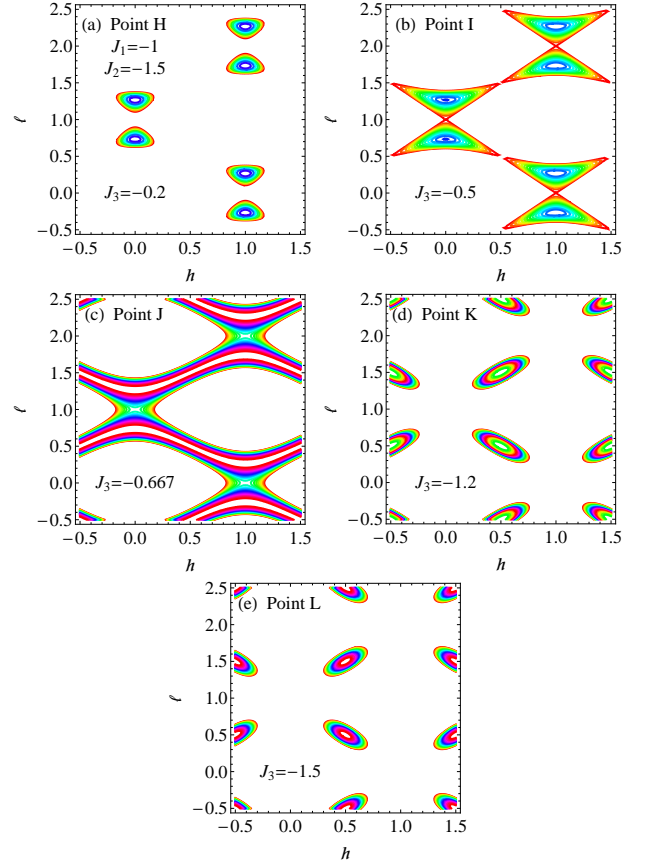
FIG. 13: (Color online) Distribution of Bragg peaks in the $(h, 0, l)$ reciprocal lattice plane. $J_1 = -1$. $J_2 = -1.5$, and J_3 is changed as a parameter. H ($J_3 = -0.2$), I ($J_3 = -0.5$), J ($J_3 = -0.667$), K ($J_3 = -1.2$), and L ($J_3 = -1.5$).
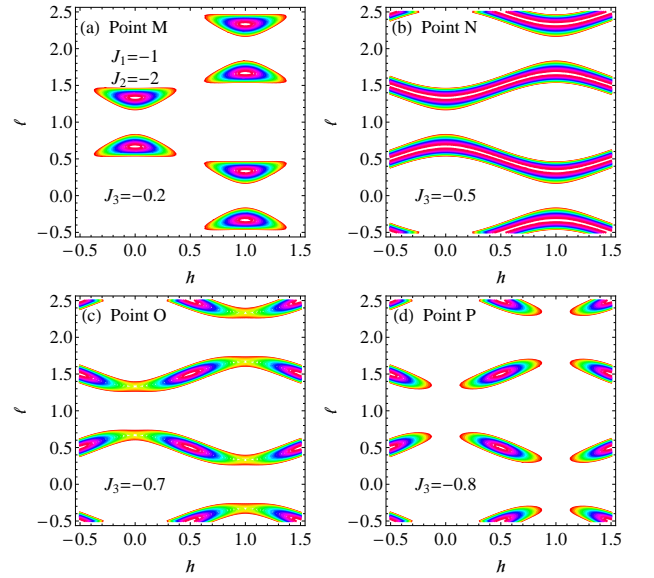
FIG. 12: (Color online) Distribution of Bragg peaks in the $(h, 0, l)$ reciprocal lattice plane. $J_1 = -1$. $J_2 = 1.5$, and J_3 is changed as a parameter. F ($J_3 = -0.5$) and G ($J_3 = -1.5$).

D. The points M, N, O, and P with $J_1 = -1.0$ and $J_2 = -2$

Typical contour plot of $(h, 0, l)$ at the points M, N, O, and P in the (J_2, J_3) phase diagram are shown in Fig. 14 The point M ($J_3 = -0.2$) is in the helical phase along the c axis. The point N ($J_3 = -0.5$) is on the phase boundary ($J_2 + J_3 = 2J_1$) between the helical phase with

FIG. 14: (Color online) Distribution of Bragg peaks in the $(h, 0, l)$ reciprocal lattice plane. $J_1 = -1$. $J_2 = -2$, and J_3 is changed as a parameter. M ($J_3 = -0.2$), N ($J_3 = -0.5$), O ($J_3 = -0.7$), and P ($J_3 = -0.8$).
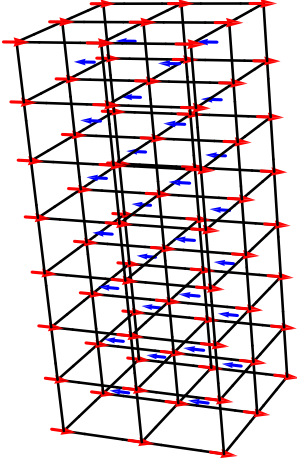
FIG. 15: (Color online) structure in the phase ($h = 0, k = 0, l = 1$).

the c axis and the phase with ($h = 1.2, k = 0, l = 1/2$). The points O ($J_3 = -0.7$) and P ($J_3 = -0.8$) are in the phase with ($h = 1/2, k = 0, l = 1/2$).

IX.   3D SPIN STRUCTURES

What is the three dimensional (3D) spin structure which is characterized with the wavevector of the magnetic Bragg peaks? The vector of spin at the site $\mathbf{R}_i$ of the real lattice space is given by

$$\mathbf{S}_i = S[\cos(\mathbf{Q} \cdot \mathbf{R}_i)\mathbf{e}_x + \sin(\mathbf{Q} \cdot \mathbf{R}_i \phi)\mathbf{e}_y]$$

where $S = 3/2$, we assume that the phase factor ϕ is equal to zero, and $\mathbf{Q}$ is defined as

$$\mathbf{Q} = (ha^*, ka^*, lc^*).$$

A.   Phase with ($h = 0, k = 0, l = 1$)

A typical spin structure for the phase with (0, 0, 1) is described in Fig. 15.

B.   Phase with ($h = 1/2, k = 0, l = 1/2$)

A typical spin structure for the phase with (1/2, 0, 1/2) is described in Fig. 16.

C.   Helical ordered phase along the c axis; $(0, 0, l_{max})$

The value l_{max} is obtained as 0.703= 5/7 – 0.0112857 for $J_2 = -1.67959$, since
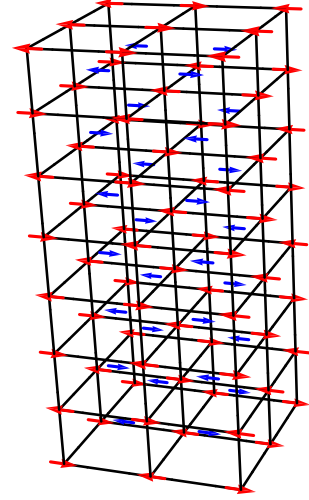
$$\cos(\pi l_{\max}) = -\frac{J_1}{J_2}.$$

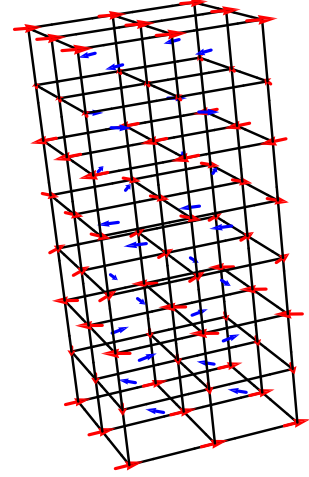FIG. 16: (Color online) Spin structure in the phase ($h = 1/2, k = 0, l = 1/2$).

FIG. 17: (Color online) Incommensurate spin structure for the helical order along the c axis with the phase (0, 0, 0.703).

A typical spin structure is incommensurate with the lattice structure and described by Fig. 17.

D.   Helical ordered phase along the c axis (Yoshimori); commensurate structure

$$\cos(\pi l_{\max}) = -\frac{J_1}{J_2},$$

with $l_{max} = 5/7 = 0.71429$. A typical spin structure is commensurate with the lattice structure and described by Fig. 18. The magnetic unit cell along the c axis is seven times larger than the unit cell of the crystal unit cell.
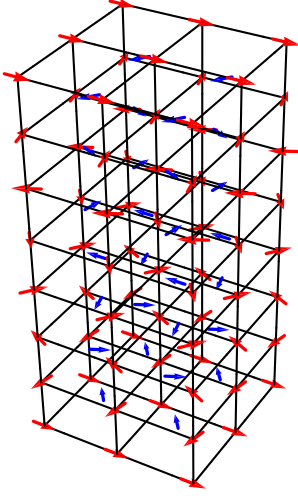
FIG. 18: (Color online) Commensurate spin structure for the helical order along the c axis. with the phase $(0, 0, 5/7)$, which is proposed by Yoshimori.
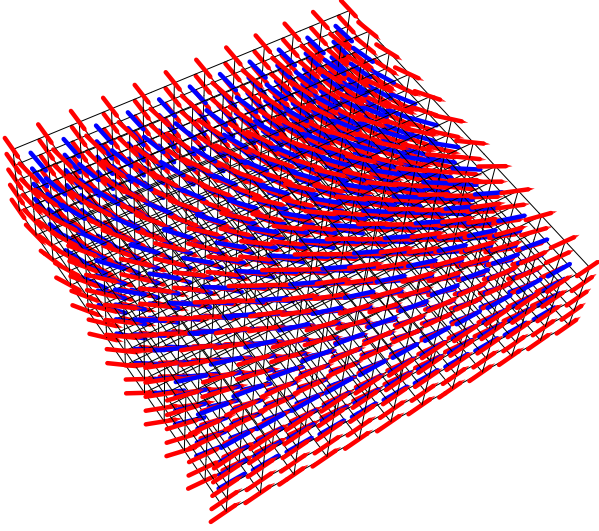

FIG. 19: (Color online) Spin structure for the helical order along the a axis with $(h_{max} = 2/3, 0, 1)$. $J_1 = -1$, $J_3 = -2.0$.

E. Helical ordered phase along the a axis: $(h_{max}, 0, 1)$

When $J_3 = -2.0$ and $J_1 = -1$, h_{max} is equal to 2/3, since

$$\cos(\pi h_{\max}) = -\frac{J_1}{J_3}.$$
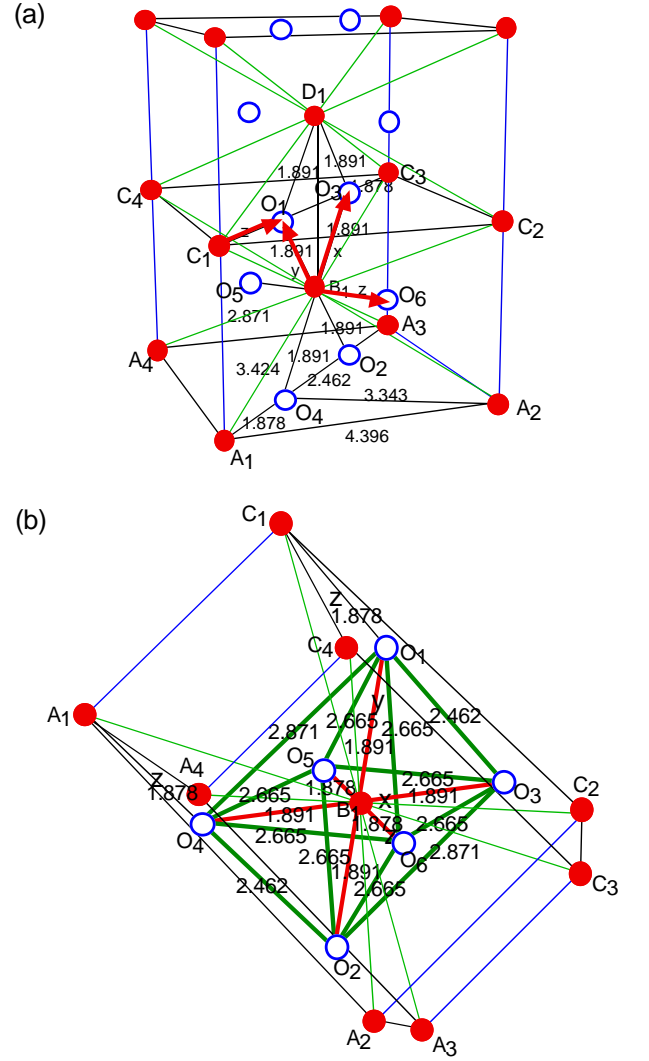
Then a typical spin structure is described by Fig. 19.

FIG. 20: (Color online) (a) Crystal structure of β-MnO$_2$. $\angle A_1 O_4 B_1 = \angle C_1 O_1 B_1 = 130.62°$. $\angle A_1 O_4 A_2 = 111.60°$. $\angle B_1 O_3 D_1 = 98.77°$. The distance (in the units of Å) is denoted by numerical value. (b) Distorted octahedra of β-MnO$_2$. $\angle O_1 B_1 O_4 = 98.77°$, $\angle O_1 B_1 O_3 = 81.225°$, $\angle O_5 O_1 O_6 = 89.590°$, $\angle O_1 O_6 O_5 = 45.205°$, and $\angle O_1 B_1 O_5 = \angle O_4 B_1 O_5 = 90.0°$ The distance (in the units of Å) is denoted by numerical value.

X. DISCUSSION: NATURE OF EXCHANGE INTERACTIONS IN THE RUTILE-TYPE β-MnO$_2$

We show that the magnetic phase diagram with $J_1 = -1$ is uniquely determined by the combination of J_2 and J_3, where the sign of J_3 is mainly negative and the sign of J_2 is changed between negative to positive. For β-MnO$_2$, we have $p_2 = 1.68469$ and as $p_3 = 0.537$, leading to $J_2 = -1.68469$ and $J_3 = -0.537$ when $J_1 = -1$. This point (J_2, J_3) for β-MnO$_2$ is in the helical order along the c axis, as shown in the magnetic phase diagram (Fig. 6).

In Fig. 20(a), we show the structure of β-MnO$_2$. Figure 20(b) shows the distorted octahedron where one Mn^{4+}

ion (cation) at the point B_1, is surrounded by six O^{2-} ions (anion) at the points O_1, O_2, O_3, O_4, O_5, and O_6. The cation-cation separation (A_1C_1, B_1D_1) along a [001] axis is considerably smaller ($2.871\mathring{A}$). Because of the distorted octahedron formed by O^{2-} ions in the vicinity of Mn^{4+} ion, the ground orbital state of Mn^{4+} ion ($3d^3$, $L = 3$ and $S = 3/2$) is split into the t_{2g} ($d\epsilon$) level [lower energy level, triple degenerate; $d(xy)$, $d(yz)$, and $d(zx)$ states] and the e_g ($d\gamma$) level (upper energy, double degenerate;$d(3z^2 - r^2)$, $d(x^2 - y^2)$). The t_{2g} state is occupied by three electrons with spin up state $|+\rangle$. The ϵ_g state is empty. As a result, the ground state is orbital singlet, indicating that the orbital angular momentum is quenched. In β-MnO_2, the e_g electrons are responsible for the metallic conduction, while the localized t_{2g} electrons are responsible for the magnetism. In Fig. 20(b), the $(3z^2 - r^2)$ orbital axis at the point B_1 coincides with $O_5B_1O_6$ (the z axis). The $d(x^2 - y^2)$ axes coincide with $O_3B_1O_4$ (the x axis) and the $O_1B_1O_2$ (the y axis). The x and y axes are perpendicular to the z axis. However, the x axis is not perpendicular to the y axis ($98.78°$, $81.22°$).

A.   Origin of the direct exchange interaction J_2

We consider the exchange interaction J_2 between the points, B_1 and D_1 (or between the points A_1 and C_1). The distance B_1D_1 (A_1C_1) is $2.871\mathring{A}$. In Fig. 20(b), one $d(xy)$ orbital (t_{2g}) from the point B_1 bisects the angle $\angle O_1B_1O_3$ and meets at the middle point of the edge O_1O_3. The other $d(xy)$ orbital from the point D_1 (the center of neighboring octahedron) bisects the angle $\angle O_1D_1O_3$ and meets at the middle point of the edge O_1O_3. According to Goodenough,[11] the predominant interactions between neighboring cations whose cation-ccupied octahedra share an edge, are assumed to be direct cation-cation exchange interaction. Thus the interaction J_2 is antiferromagnetic (Heitler-London type) for β-MnO_2.

B.   Origin of superexchange interaction J_1

We consider the interaction between Mn^{4+} at the point B_1 and the Mn^{4+} at the point C_1 as shown in Fig. 20, where the distance C_1B_1 is $3.424\mathring{A}$. According to Goodenough,[11] this interaction (J_1) is a superexchange one since the cation-occupied octahedra share a common corner (point O_1). The angle $C_1O_1B_1$ is equal to $130.62°$, this interaction is antiferromagnetic for β-MnO_2. According to Goodenough,[11] when the cation-occupied octahedral share a common corner, there can be no direct overlap of neighboring cation orbitals and therefore there is no cation-cation interactions.

What is the origin of J_1? The point C_1 is the center of the neighboring octahedron. The direction of C_1O_1 is the z axis of this octahedron. A p orbital of O_1 is expected to be directed toward C_1 (p_σ orbital) so as to overlap the $d(3z^2 - r^2)$ orbital of the point C_1, where the p orbital (p_x, p_y, p_z state) is called as p_σ orbital when the principal axis of the p orbital coincides with the direction of the bond. A partial covalent bond between the $d(3z^2 - r^2)$ orbital and the p_σ orbital can be formed. Then the charge transfer occurs from the p_σ orbital with the spin-up state $|\uparrow\rangle$ to the ϵ_g state. Consequently, the spin of Mn^{4+} at the point C_1 is still in the spin-up state, while the resulting spin of O^{2-} at the point O_1 is in the spin-down state. The remaining p_σ state at the point O_1 is magnetically coupled with the t_{2g} state of the Mn^{4+} at the point B_1. When this coupling (denoted as K_0) is antiferromagnetic, then the suprexchange interaction between Mn^{4+} at the point C_1 and Mn^{4+} at the point B_1 is ferromagnetic. On the other hand, when this coupling K_0 is ferromagnetic, then the superexchange interaction between Mn^{4+} at the point C_1 and Mn^{4+} at the point B_1 is antiferromagnetic. Here we note that the angle $\alpha = \angle C_1O_1B_1$ is equal to $130.62°$ for β-MnO_2, which is very different from $90°$. If $\alpha = 90°$, the p_σ orbital on the bond O_1C_1 coincides with the p_π orbital on the bond O_1B_1 (the y axis), where the p orbital (p_x, p_y, p_z state) is called as p_π orbital when the principal axis of the p orbital is perpendicular to the direction of the bond. The p_π orbital is coupled with the t_{2g} state of the Mn^{4+} at the point B_1, since the ϵ_g state is empty. According to the Goodenough-Kamamori-Anderson rule,[11–14] the interaction K_0 is antiferromagnetic, since the p_π orbital is not orthogonal to the t_{2g} orbital. If $\alpha = 180°$, the p_σ orbital is coupled with the t_{2g} orbital of the Mn^{4+} at the point B_1 the interaction K_0 is ferromagnetic, since the p_σ orbital is orthogonal to the t_{2g} orbital.

The sign of K_0 is dependent on the value of α. There may be a critical angle α_c. K_0 is ferromagnetic for $\alpha > \alpha_c$ and K_0 is antiferromagnetic for $\alpha < \alpha_c$. Experimentally, the superexchange interaction J_1 is antiferromagnetic for β-MnO_2, which means that K_0 is ferromagnetic. The critical angle α_c is lower than $130.62°$.

The direct cation-cation exchange interaction (J_2) is expected to be stronger than the superexchange interactions J_1 The competition between J_1 and J_2 can lead to a complicated compromise magnetic order; $J_2/J_1 = 1.68469$ for β-MnO_2. Note that the discussion of Osmond[15] on the nature of J_2 may be inappropriate.

C.   Origin of superexchange interaction J_3

We consider the interaction between Mn^{4+} at the point A_1 and the Mn^{4+} at the point A_2, as shown in Figs. 20(a) and (b), where the distance A_1A_2 is $4.396\mathring{A}$. According to Goodenough,[11,12] this interaction (J_3) is a superexchange one (cation-anion-cation) since the cation-occupied octahedra share a common corner (point O_4). The angle $\angle A_1O_4A_2$ is equal to $\alpha = 111.60°$, the distance O_4A_2 is $3.343\mathring{A}$, and the distance O_4A_1 is $1.878\mathring{A}$. This interaction is experimentally antiferromagnetic for β-MnO_2; $p_3 = J_3/J_1 = 0.537$. This means that the crit-

ical angle α_c is between 90° and 111.60°.

XI. CONCLUSION

We have studied the magnetic phase diagram of (J_2 vs J_3) with $J_1 = -1$ in the rutile type β-MnO$_2$ by using the equi-energy contour plot. The distribution of the magnetic Bragg peaks can be clearly visualized. The magnetic phase diagram consists of the multicritical point (the intersection $J_2 J_3 = J_1^2$ and $J_2 + J_3 = 2J_1$), the helical order along the c axis, the $(h = 1/2, k = 0, l = 1/2)$ phase, the helical order along the a axis, and the phase $(h = 0, k = 0, l = 1)$. The phase transition is of the first order between the $(h = 1/2, k = 0, l = 1/2)$ phase and the helical order along the c axis, and between the $(h = 1/2, k = 0, l = 1/2)$ phase and the helical order along the a axis. The phase transition is of the second order between the phase $(h = 0, k = 0, l = 1)$ and the helical order along the c axis, and between the phase $(h = 0, k = 0, l = 1)$ and the helical order along the a axis.

Acknowledgments

* suzuki@binghamton.edu
† itsuko@binghamton.edu
[1] R.A. Erickson, Phys. Rev. **90**, 779 (1953).
[2] A. Yoshimori, J. Phys. Soc. Jpn. **14**, 807 (1959).
[3] N. Ohama and Y. Hamaguchi, J. Phys. Soc. Jpn. **30**, 1311 (1971).
[4] M. Regulski, R.Przenioslo, I. Sosnowska, and J.-U. Hoffmann, Phys. Rev. B **68**, 172401 (2003).
[5] M. Regulski, R.Przenioslo, I. Sosnowska, and J.-U. Hoffmann, J. Phys. Soc. Jpn.**73**, 3444 (2004).
[6] H. Sato, K. Wakiya, T. Enoki, T. Kiyama, Y. Wakabayashi, H. Nakano, and Y. Murakami, J. Phys. Soc. Jpn. **70**, 37 (2001).
[7] H. Sato, Y. Kawamura, T. Ogawa, Y. Murakami, H. Ohsumi, M. Mizumaki, and N. Ikeda, Physica B **329 − 333**, 757 (2003).
[8] H. Sato, T. Enoki, M. Isobe, and Y. Ueda, Phys. Rev. B **61**, 3563 (2000).
[9] T. Nagamiya, *Solid State Physics*, edited by F. Seiz, D. Turnbull, and H. Ehrenreich, **20**, 305 (Academic Press, New York,1967).
[10] H. Bizette and B. Tsai, Colloque sur la polarization de la matere cited by Lidiard (Paris, C.N.R.S., 1949) 164, Reports on Progr. in Phys. **17**, 201 (1954).
[11] J.B. Goodenough, Phys. Rev.**117**, 1142 (1960).
[12] J.B. Goodenough, *Magnetism and the Chemical Bond* (John-Wiley & Sons, New York, 1963).
[13] J. Kanamori, J. Phys. Chem. Solid **10**, 87 (1959).
[14] P.W. Anderson, *Solid State Physics*, edited by F. Seiz and D. Turnbull (Academic Press, New York and London, 1963) **14**, 99.
[15] W.P. Osmond, Proc. Phys. Soc. **87**, 335 (1966).